Respiratory Physiology & Neurobiology 185 (2013) 625–638

Contents lists available at SciVerse ScienceDirect

Respiratory Physiology & Neurobiology

journal homepage: www.elsevier.com/locate/resphysiol

# A first principles calculation of the oxygen uptake in the human pulmonary acinus at maximal exercise

A. Foucquier[a], M. Filoche[a,b], A.A. Moreira[c], J.S. Andrade Jr.[c], G. Arbia[a,b], B. Sapoval[a,b,*]

[a] Physique de la Matière Condensée, CNRS, Ecole Polytechnique, 91128 Palaiseau, France
[b] Centre de Mathématiques et de leurs Applications, CNRS, UniverSud, 94235 Cachan, France
[c] Departamento de Física, Universidade Federal do Ceará, Fortaleza, Brazil

ARTICLE INFO

*Article history:*
Accepted 26 October 2012

*Keywords:*
Gas exchange
Exercise
Diffusion limitation
Acinus
Alveolar gas
Membrane permeability

ABSTRACT

It has recently been shown that the acinus can have a reduced efficiency due to a "screening effect" governed by the ratio of oxygen diffusivity to membrane permeability, the gas flow velocity, as well as the size and configuration of the acinus. We present here a top to bottom calculation of the functioning of a *machine acinus* at exercise that takes this screening effect into account. It shows that, given the geometry and the breathing dynamics of real acini, respiration can be correlated to a single equivalent parameter that we call the *integrative permeability*. In particular we find that both $\dot{V}_{O_2,max}$ and $PA_{O_2}$ depend on this permeability in a *non-linear* manner. Numerical solutions of dynamic convection–diffusion equations indicate that only a narrow range of permeability values is compatible with the experimental measurements of $PA_{O_2}$ and $\dot{V}_{O_2,max}$. These permeability values are significantly smaller than those found in the literature. In a second step, we present a new type of evaluation of the diffusive permeability, yielding values compatible with the top to bottom approach, but smaller than the usual morphometric value.



## 1. Introduction

Gas exchange in the pulmonary acinus involves different physicochemical phenomena occurring in a dynamical and complex geometry. The global process includes five main steps (Weibel, 1984): (i) air convective flow; (ii) oxygen diffusion in air; (iii) diffusion through membrane and plasma; (iv) diffusion inside the red blood cells; and finally, (v) oxygen binding to hemoglobin.

In order to understand how these phenomena combine to govern respiration at exercise, we study in some detail how the steps (i) convection, (ii) oxygen diffusion through air, and (iii) diffusion through membrane and plasma interact within the dynamic of the acinus tree structure. The physiological problem that we quantitatively investigate is schematically represented in Fig. 1. In this problem, the acinus morphology plays an essential role: the gas exchange units are arranged serially along the branched alveolar ducts, which direct $O_2$ toward the peripheral units while the capillary network units are arranged in parallel.

During each breathing cycle, the proximal acinar regions always receive fresh air while the more distal regions located deeper are only fed by diffusion. The transition between convection-dominated and diffusion-dominated regions therefore moves back and forth periodically, constantly modifying the size of the diffusion cell. The time-dependent diffusion cell regions may be subjected to diffusion limitations also called *diffusion screening*. Diffusion screening is the consequence of the fact that, when $O_2$ molecules diffuse inside the acinus, they may cross the alveolar membrane and be trapped by the blood. As the gas continues deeper into the acinus, this process causes the progressive transfer of $O_2$ into the blood. This results in a gas that is depleted of part of its oxygen content in the peripheral region.

In early studies, incomplete gas mixing was already assigned to the finite diffusivity of oxygen, preventing it to evenly spread in the acinus within an inspiration (Scheid and Piiper, 1980). In this frame, the possible non-uniformity of the oxygen concentration was called stratification. The fact that the distribution of $O_2$ partial pressure could present a gradient was also indicated in (Weibel et al., 1981). The resolution of the best NMR experimental measurements, with pixels of order 6 mm in size, is insufficient to show concentration gradients within the scale of an acinus (Miller et al., 2010). Lacking direct measurements of the distribution of oxygen concentration, the respective roles of convection and diffusion in the gas mixing process were examined through numerical simulations (Paiva and Engel, 1985, 1987; Dutrieue et al., 2000; Tawhai and Hunter, 2001). These studies showed that concentration gradients might exist as a consequence of efficient capture of oxygen by hemoglobin, the permeability of the alveolar membrane being considered in these models as infinite. In sharp contrast with the previous works, we

* Corresponding author. Tel.: +33 169334725.
*E-mail address:* bernard.sapoval@polytechnique.edu (B. Sapoval).

1569-9048/$ – see front matter © 2012 Elsevier B.V. All rights reserved.
http://dx.doi.org/10.1016/j.resp.2012.10.013

**List of symbols**

| | |
|---|---|
| $a$ | radius of a spherical blood cell |
| $\alpha$ | partition ratio (solubility) of oxygen in the alveolar membrane and plasma compared with the gas |
| $\alpha'$ | partition ratio (solubility) of oxygen in an erythrocyte compared with plasma |
| $\delta$ | dilation amplitude |
| $C_g$ and $C_L$ | oxygen concentrations in the alveolar gas and in the membrane–plasma liquid |
| $D$ | diffusion coefficient of oxygen into air |
| $D_{O_2,H_2O}$ | diffusion coefficient of oxygen into water |
| $D_M$ | membrane conductance |
| $D_e$ | erythrocyte conductance |
| $DL_{O_2}$ | lung diffusive capacity for oxygen |
| $k(t)$ | acinus linear dilation factor |
| $K$ | Krogh permeability |
| $PA_{O_2}$ | average oxygen partial pressure in the acinus |
| $PI_{O_2}$ | oxygen partial pressure at the entrance of the acinar tree |
| $Pv_{O_2}$ | oxygen partial pressure in the venous blood |
| $Pc_{O_2}$ | mean oxygen partial pressure in the capillaries, used in the Bohr equation |
| $Pa_{O_2}$ | oxygen partial pressure in arteries |
| $Palv_{O_2}(r,t)$ | local oxygen partial pressure in the acinar space at position $r$ and time $t$ |
| $V_{ac}$ | outer acinar volume |
| $SA_{lung}$ | total lung alveolar surface |
| $Sc_{lung}$ | total lung capillary surface |
| $SAc_{lung}$ | surface of a single acinus |
| $\tau_{hb}$ | equivalent diffusion length (harmonic mean of the distances between alveolar space and erythrocytes) |
| $\tau_I$ | duration between the beginning of inspiration and the arrival of fresh air into the acinus |
| $\theta_{O_2}$ | reaction rate of hemoglobin for oxygen |
| $U(r,t)$ | convection velocity of air at position $r$ and time $t$ |
| $V_c$ | capillary volume |
| $\dot{V}_{O_2,max}$ | oxygen consumption |
| $W$ | "true" diffusive permeability of the membrane and plasma |
| $W_M$ | morphometric membrane permeability |
| $W_e$ | erythrocyte permeability |
| $W_{eq}$ | global permeability (according to the formulation of Roughton and Forster) |
| $\Omega$ | integrative permeability (according to our model) |

will find herein that a finite membrane resistance is a key parameter in understanding the overall oxygen transport.

In a *steady state regime* description of respiration, quantitative screening effects essentially depend on two characteristic length scales of the system, one physicochemical and the other geometrical. The physicochemical characteristic is a length called $\Lambda_{O_2}$, which is the ratio of the diffusion coefficient of oxygen in air $D$ to the membrane permeability to oxygen $W$ ($W$ being the response to a concentration difference, expressed in cm/s). The geometrical characteristic is the "surface perimeter" $L_p$: it corresponds to the average length of a two-dimensional planar cut of the surface (Sapoval, 1994a,b; Sapoval et al., 2001). It has been shown that when $\Lambda_{O_2}$ is much larger than $L_p$ the surface works uniformly. On the other hand, when $L_p$ is larger than $\Lambda_{O_2}$, oxygen cannot reach the less accessible regions and in consequence, the surface is only partially active. In the human lung, the physicochemical length $\Lambda_{O_2}$ is equal to 28 cm if one uses the admitted value of the membrane permeability; the morphometric study of the human acinus yields a value

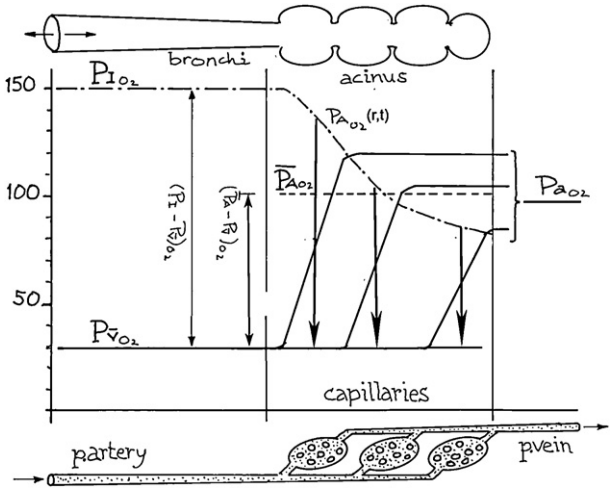


**Fig. 1.** Qualitative schematic of the problem that is solved numerically here: profile of $O_2$ partial pressures along the airway tract *during inspiration*, and along the perfusion pathway from the pulmonary artery to the capillary units and the pulmonary vein. The gas exchange units corresponding to the capillary units are perfused in parallel but ventilated in series. The input partial pressures $PI_{O_2}$ and the capillary partial pressure are modulated in the acinar gas exchanger in a mutually dependent manner. *During expiration* this schematic is not valid as the regions richer in oxygen are rapidly depleted.
Courtesy of E. R. Weibel.

of $L_p$ of about 30 cm for a 1/8 subacinus. The remarkable agreement for several mammalian species between the value of $\Lambda_{O_2}$, a *purely physicochemical* length, and the value of $L_p$, the *purely morphological* perimeter of the acini, strongly suggests that diffusion screening in the gas might play a role in mammalian respiration (Sapoval et al., 2001, 2002a,b; Felici et al., 2003, 2004, 2005; Grebenkov et al., 2005; Weibel et al., 2005; Hou et al., 2010; Mayo et al., 2012).

The present work shows however that the description of the steady state regime has to be profoundly revised in order to properly account for the role of cyclic respiration. This role has already been studied by Paiva and Engel (1985) in a bottom-up approach. In their approach the final transfer was only depending on the hemoglobin trapping resistance, neglecting the resistance due to diffusion across the membrane and plasma. In a very recent work, Swan and Tawhai (2011) also used a bottom-up approach to numerically compute the advective and diffusive oxygen transport assuming the usual description of oxygen trapping by blood. They found that the heterogeneity of oxygen partial pressure was reduced as compared to that found in the above papers in which only the usual morphometric value of the diffusive resistance was considered.

Here we first develop a top to bottom approach by computing the behavior of a "machine acinus" and try to find *under which conditions this machine works like the real acinus*. This "machine acinus" possesses the geometry and the dynamics of the real acinus, but its effective permeability is a priori *unknown*. The goal here is to determine the necessary value of this permeability that accounts for both observed values of maximum oxygen consumption $\dot{V}_{O_2,max}$ and average $O_2$ acinar partial pressure $PA_{O_2}$ respectively. As a result of our numerical studies, we found a value of the permeability significantly smaller than the one generally accepted. This single permeability value allows one to accurately calculate the oxygen capture for athletes at peak exercise. In other words, we show that athlete's acini work at peak exercise like our "machine acini".

The reason for the difference in the new permeability value, calculated here, as opposed to the previously accepted value is explored on the basis of the dynamics of saturation. Using the old

value based on the morphology approach results in a contradiction in the time dependence of blood saturation. We then propose a new bottom-up approach to correct the purely diffusive component of the permeability.

The net result of this work is that the top to bottom and the bottom up approaches, *although based on totally different concepts*, give very close values.

## 2. Methods: top to bottom

### 2.1. The concept of a "machine acinus"

During respiration, both alveolar and capillary oxygen partial pressures vary in space and time and are not directly measurable quantities. Furthermore, as shown in the literature and below, a uniform oxygen partial pressure transversally to the capillary vessel during oxygen transfer cannot exist. At the acinus level, the situation is represented in Fig. 1. It displays at a given time the pressure profile along the ventilation pathway from the conducting airways into the acinus, as well as in relation to the perfusion of the capillary gas exchange units that are arranged along the acinar airways. It shows that the gas exchange units are perfused in parallel but ventilated in series. In the gas phase, $PI_{O_2}$ is maintained near the entry of the acinus during a part of inspiration (see below) and then gradually decreases in space as $O_2$ is absorbed. It is important to remember that the number of alveoli doubles with each generation in the acinus so that the vast majority is located in the terminal generations that are particularly affected by diffusion screening (Weibel et al., 2005; Haefeli-Bleuer and Weibel, 1988).

Very generally, the entire oxygen transport in the acinus (from the transitional bronchiole to the blood) involves three different characteristic scales. The first scale, of the order of a centimeter, corresponds to the spatial variations of the oxygen partial pressure in the acinar airways. The second scale, slightly smaller than one millimeter, corresponds to the typical contact length between a capillary and the alveolar membranes. The last scale, of the order of a few micrometers, is the diameter of the capillary or the typical size of the red blood cells. From the engineering point of view proposed here, the second scale is considered very small compared to the first. Consequently, the oxygen exchange can be modeled by a point-wise boundary condition: At each point $r$ of the alveolar surface the entire exchange process is described by a small *black box* whose driving forces are respectively $Palv_{O_2}(r,t)$, the oxygen partial pressure at point $r$ and time $t$, and $Pv_{O_2}$, the venous oxygen partial pressure (Fig. 1). The oxygen flow rate through a surface element $ds$ at location $r$ and time $t$ is equal to:

$$d\Phi(r,t) = \Omega \times (Palv_{O_2}(r,t) - Pv_{O_2}) \tag{1}$$

where $\Omega$ is a quantity that we call *integrative permeability*. In that engineering picture, $\Omega$ accounts for all the complexity of the oxygen diffusion across the alveolar membrane, the diffusion through the plasma, and the blood equilibration saturation.

This integrative permeability $\Omega$ can also be interpreted as the value one should assign to the membrane permeability in order to recover the values of $PA_{O_2}$ and $\dot{V}_{O_2,max}$, *assuming that the blood acts as a perfect sink* (i.e. with neither hemoglobin resistance nor blood saturation). From the physical point of view implemented here, the relation between the integrative permeability $\Omega$ and the capillary equilibration is considered to pertain to a *black box* to be opened later. Eq. (1) was used in a preliminary calculation of the dynamics of the flux (Filoche et al., 2008), but without considering the value of $PA_{O_2}$ necessary to permit blood saturation.

In the following, the geometrical and dynamical properties of an average acinus are considered to be known, and we look for the values of the integrative permeability $\Omega$ that allows us to simultaneously explain both $\dot{V}_{O_2,max}$ and $PA_{O_2}$ values (Astrand et al., 2003).

### 2.2. The convection–diffusion–permeation equations

Away from the alveolar surface, the oxygen partial pressure at any point $\vec{r}$ within the acinus volume and at time $t$ obeys the convection–diffusion equation:

$$\frac{\partial Palv(\vec{r},t)}{\partial t} - D\Delta Palv(\vec{r},t) + \vec{\nabla}.(Palv(\vec{r},t)\vec{U}(\vec{r},t)) = 0 \tag{2}$$

where $D$ is the oxygen diffusion coefficient in air ($0.20\,cm^2/s$) and $U(r,t)$ is the gas velocity at $\vec{r}$ and $t$.

On a point of the alveolar surface, the boundary condition can be written by equating the flux of oxygen across the alveolar membrane, obtained from Eq. (1), and the flux of oxygen coming from the bulk, derived from Eq. (2):

$$D\frac{\partial Palv(\vec{r},t)}{\partial n} = \Omega \times (Palv_{O_2}(\vec{r},t) - Pv_{O_2}) \tag{3}$$

The total flux of oxygen from air to blood during a period of time can be expressed as:

$$\Phi = \iiint \Omega(Palv(\vec{r},t) - Pv_{O_2})ds_{alv}dt. \tag{4}$$

The quantity $PA_{O_2}$ is defined here by the space average:

$$PA_{O_2}(t) = \frac{1}{V_{ac}}\iiint Palv(\vec{r},t)dV \tag{5}$$

As the radius of an acinar duct and the size of an alveolus are each about 0.025 cm, the diffusion time of $O_2$ from the duct into the alveolus is of the order of 1–2 ms, a time shorter that the drift duration on a alveolus size and negligible compared to the duration of a respiratory cycle. This justifies that we use a simplified model of the acinus described as a one-dimensional tree (Paiva and Engel, 1985; Felici et al., 2004, 2005), each branch of this tree being described as a 1D channel. The gas exchange with blood occurs at the surface of the channel while transport takes place along the channel both by diffusion and convection.

For each acinar branch, a one dimensional convection–diffusion permeation equation has to be solved:

$$\frac{\partial Palv(x,t)}{\partial t} = D\frac{\partial^2 Palv(x,t)}{\partial x^2} - \frac{\partial}{\partial x}(Palv(x,t)U(x,t)) - \Omega\left(\frac{S_{br}(x,t)}{V_{br}(x,t)}\right)[Palv(x,t) - Pv] \tag{6}$$

where $x$ is the position along the branch and $U$ is the absolute velocity of the air, and the ratio $(S_{br}/V_{br})$ measures the exchange surface to volume ratio of the branch.

Boundary conditions at the acinus entrance are different during inspiration, when outside air is brought to the acinus entrance, and expiration when the gas present in the acinus is expelled, the proximal regions being expelled at high velocity.

During inspiration there exists a finite time $\tau_I$ during which the gas reaching the acinus entrance is the dead space gas (Florens et al., 2011). The time $\tau_I$ is about 0.1 s at exercise. The oxygen partial pressure at the acinus entrance $PI_{O_2}$ is assumed to be constant from time $t = \tau_I$ until half of the ventilation cycle time $T$:

$$P(0,t) = PI_{O_2}k \quad \text{for} \quad \tau_I \le t \le T/2 \quad \text{when} \quad U(0,t) \ge 0 \tag{7}$$

During exhalation, the gas present in the acinus is carried away by the entrance velocity $U(x=0,t)$. So the oxygen partial pressure at the acinus entrance at time $t+dt$ is the pressure that existed in the acinus at time $t$ at a point of abscissa $dx = -U(0,t)dt$. In other

words, $P(0, t+dt) = P(-U(0,t)dt, t)$. Subtracting $P(0,t)$ on both sides and dividing by $dt$, one gets:

$$U(0,t)\frac{\partial P}{\partial x} + \frac{\partial P}{\partial t} = 0 \quad \text{for} \quad t \le \tau_I \quad \text{and} \quad t \ge T/2, \quad \text{when} \quad U(0,t) \le 0 \tag{8}$$

### 2.3. The ventilation in the acinar tree

In our calculations, ventilation is assumed to be only driven by the successive dilations and contractions of the acini. The airflow is therefore independent of the gas exchange (the gas pressure is approximately uniform inside the acinus, the oxygen uptake being essentially compensated by $CO_2$ discharge). The convection–diffusion equation is solved numerically using finite differences, each duct being discretized into 4 cells. Inside a duct, each point has two neighbors that belong to the same duct while a bifurcation point has three neighbors, one per incoming branch (see Appendix A).

At any given time, the air velocity is position dependent along each duct. The entire air velocity map is computed during the breathing cycle according to flux conservation. Ventilation is assumed to be sinusoidal so that lengths and surfaces dilate respectively as $k(t)$ and $k(t)^2$, $k(t)$ being given by:

$$k(t) = \left[1 + \delta\left(\frac{1-\cos(2\pi f t)}{2}\right)\right]^{1/3} \tag{9}$$

Here $\delta$ is the volume dilation amplitude, and $f$ is the respiratory frequency. The numerical implementation for computing the time dependent velocity map is given in Appendix B.

The value of the air pressure at the trachea is about 760 mmHg. The air that reaches the acini is saturated with water with partial pressure of about 47 mmHg. The oxygen partial pressure at the entrance of the acinus is thus $PI_{O_2} = (760-47)\times 0.21 \approx 150$ mmHg.

The volume dilation amplitude according can be calculated from the ventilation rate $\dot{V}_E$ (expressed in L/min), the breathing period $T$, and the total lung volume $V_{tot}$:

$$\delta = \frac{V_{max} - V_{min}}{V_{min}} = \frac{(\dot{V}_E T/60)}{V_{max} - (\dot{V}_E T/60)} \tag{10}$$

At exercise, the values of $\dot{V}_E$ and $T$ are 100 L/min and 2 s respectively (Weibel, 1984; Astrand et al., 2003). Given that the maximal volume $V_{max}$ attained at peak exercise is about 90% TLC, $V_{max}$ is about 5600 mL, which leads to a value of $\delta = 1.5$.

## 3. Units

Permeabilities are usually measured in standard physiological units such as ml STP per surface unit per time unit per partial pressure unit (for instance cm $min^{-1}$ $mmHg^{-1}$). In the following we will use an equivalent physical unit which measures the permeabilities in units of length divided by time, or velocity units. For example, the flux $\Phi_M$ across a permeable barrier (the flux being defined as the number of molecules per unit time per unit surface), where the *concentration* is $C_g$ (g for gas) on one side of the barrier and 0 on the other side of the barrier, can be written as $\Phi_M = C_g W$. A simple dimensional analysis shows that the permeability $W$ is measured in units of length divided by time, or velocity. Indeed, the very definition of the flux across a unit surface is $\Phi_M = C_g \bar{u}$ where $\bar{u}$ is the average particles velocity. So $W$ (in pysical unit) $= \bar{u}$, the average oxygen velocity. The usual physiological units hide the fact that the permeability really measures an average particle velocity. For example, the time to cross a distance $\delta$ is equal to $\delta/W$.

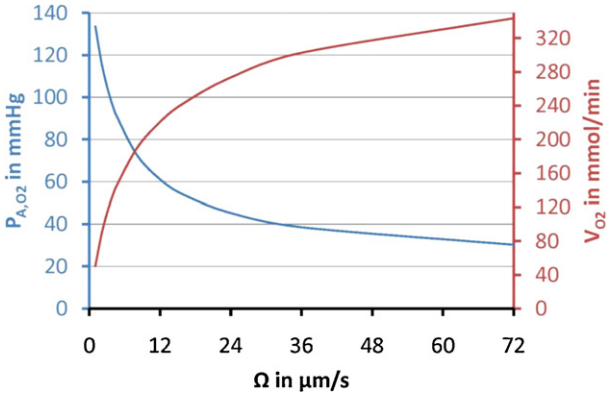


**Fig. 2.** Dependence of the oxygen uptake $\dot{V}_{O_2,max}$ and the alveolar pressure $PA_{O_2}$ at full exercise on the integrative permeability $\Omega$. The dependence is not linear due to the complex effect of the permeability value on the dynamics of diffusion-convection. The values of $\Omega$ in the circle, or range of credibility, range from 2.8 to 4.3 µ/s.

The equivalence between the physical and the physiological units is then given by: $W = 760 \cdot W_{STP}$.

### 3.1. A necessary value for the integrative permeability

Numerical simulations of the above equations (detailed in Appendix B) were run on a reference acinus of 8 generations of total volume $V_{acinus} = 187\ mm^3$ and an exchange surface of one acinus $SAc_{lung} = 3930\ mm^2$. The physiological data used for the simulations were: $Pv_{O_2} = 20$ mmHg, $\delta = 1.5$, $T = 2$ s, $\dot{V}_E = 100$ L/min, $V_{TLC} = 6.2$ L, $V_T = 3333$ mL (Weibel, 1984, p. 284); the surface-to-volume ratio in the acinus $SAc_{lung}/V$ is about 30 $mm^{-1}$ (the volume $V$ corresponds to the vital capacity equal to about 70% TLC (Astrand et al., 2003)). It accounts for the reduction of the free alveolar surface in an air-filled acinus at 40–80% TLC (Bachofen et al., 1987). $\dot{V}_{O_2,max}$ is computed assuming that the lung is made of identical acini, for a total acinar volume of about 6 L.

Once these parameters are fixed, the total flow and the mean oxygen partial pressure (averaged over space and time) only depend on the integrative permeability $\Omega$, or, more precisely, its product with the alveolar surface. We have then calculated the distribution in space and time of the pressure and the flow for several *arbitrary* values of $\Omega$, ranging from 1 µm/s to 72 µm/s.

A striking result of our calculation is shown in Fig. 2: one can observe that $\dot{V}_{O_2,max}$ *is not proportional to the integrative permeability*. From $\Omega = 72$ µm/s to $\Omega = 3.5$ µm/s, the permeability is divided by about 21 while the oxygen uptake $\dot{V}_{O_2,max}$ is only divided by about 2.7. This is a consequence of the diffusion screening in a changing convection–diffusion–permeation tree. For large enough permeabilities, oxygen is absorbed in the proximal regions and a large fraction of the acinus surface is inactive. A diminution of the permeability results in a progressively larger fraction of the surface being active for transfer, until the entire surface is utilized. This compensation mechanism disappears when the total surface is used. The marked dependency of the flow for small permeabilities corresponds to the classical fact that a pathologic decrease of these factors (by edema or emphysema) directly impairs the oxygen consumption at exercise, in contrast with the rest situation (Sapoval and Filoche, 2008).

Table 1

The average $PA_{O_2}$ is also displayed in Fig. 2 and exhibits a nonlinear behavior. The integrative permeability entirely determines the functioning of the machine acinus (see Table 2). The question then is: are there values of $\Omega$ compatible with experimental

**Table 1**
Geometrical parameters of the acinar tree: per generation the length, the inner and outer diameter and the total alveolar surface. We can see that on the three first generations the inner diameter is larger due to the fact the alveoli do not cover the whole duct.

| Generation | Length (mm) | Inner diameter (mm) | Outer diameter (mm) | Alveolar surface ($mm^2$) |
|---|---|---|---|---|
| 0 | 0.8 | 0.498 | 0.736 | 2.5 |
| 1 | 1.330 | 0.497 | 0.694 | 16.7 |
| 2 | 1.118 | 0.492 | 0.686 | 41.4 |
| 3 | 0.930 | 0.397 | 0.700 | 74.8 |
| 4 | 0.832 | 0.382 | 0.711 | 158.5 |
| 5 | 0.671 | 0.356 | 0.684 | 253.0 |
| 6 | 0.692 | 0.335 | 0.694 | 479 |
| 7 | 0.716 | 0.311 | 0.708 | 873 |
| 8 | 1.167 | 0.258 | 0.701 | 1563 |

$\dot{V}_{O_2,max}$ and $PA_{O_2}$? In order to find this value one can plot on the same graph $\dot{V}_{O_2,max}$ and $PA_{O_2}$ for various values of $\Omega$ (now an implicit variable) as shown in Fig. 3. We have indicated on this graph the range of credibility values of for both $PA_{O_2}$ (95–110 mmHg) and $\dot{V}_{O_2,max}$ (110–150 mmol/min) (West, 2008). Remarkably, only a narrow range of $\Omega$ values, between 2.8 and 4.3 μm/s, allows to simultaneously obtain both experimental $\dot{V}_{O_2,max}$ and $PA_{O_2}$ in the experimental credibility interval. We choose $\Omega = 3.5$ μm/s as an average value.

The distribution in space and time of the local oxygen partial pressure is shown in Fig. 4 for a value $\Omega = 3.5$ μm/s. One observes

**Table 2**
Values of $PA_{O_2}$ and $V_{O_2,max}$ computed for different values of the integrative permeability $\Omega$. For $\Omega$ around 3.5 μm/s, the computed values correspond to the ones measured in vivo for a healthy lung (which are height, weight, gender and age depend ent): $V_{O_2,max} = 110–150$ mmol/min and $PA_{O_2} \approx 95–110$ mmHg. In green, results for the morphometric diffusive permeability $W_M$, in blue, results for the usual $W_{eq}$ and in red, the results compatible with physiological measurements.

| $\Omega$ (μm/s) | $P_{A\,O2}$ (mmHg) | $\dot{V}_{O2,max}$ (mmol/min) |
|---|---|---|
| 72 | 30 | 344 |
| 36 | 38 | 303 |
| 24 | 45 | 273 |
| 16 | 54 | 243 |
| 12 | 61 | 221 |
| 8 | 73 | 189 |
| 4.4 | 92 | 142 |
| 4.2 | 94 | 138 |
| 4 | 96 | 135 |
| 3.8 | 97 | 131 |
| 3.6 | 99 | 127 |
| 3.5 | 100 | 125 |
| 3.4 | 101 | 123 |
| 3.2 | 103 | 118 |
| 3 | 105 | 113 |
| 2.8 | 107 | 109 |
| 2.6 | 109 | 103 |
| 2.4 | 112 | 98 |
| 2.2 | 114 | 92 |
| 2 | 117 | 86 |
| 1 | 134 | 51 |

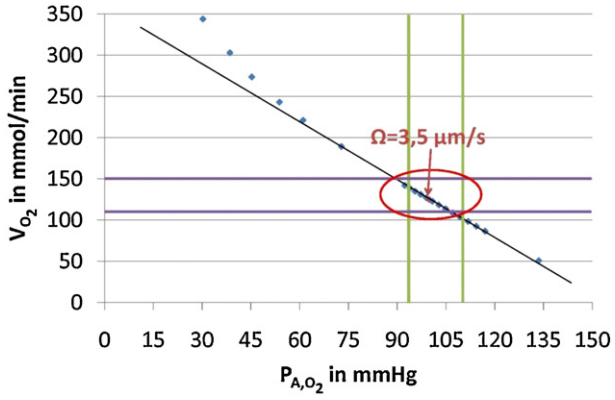


**Fig. 3.** Determination of the necessary value of the permeability. The figure presents a plot of the oxygen flux $\dot{V}_{O_2,max}$ as a function of the average partial pressure using the various values of the integrative permeability $\Omega$ as an implicit parameter. The value $\Omega = 3.5$ μm/s permits at the same time to recover *both* known values for $\dot{V}_{O_2,max}$ and $PA_{O_2}$.

that the pressure is far from uniform in space or time during the respiratory cycle. It is interesting to note that the oxygen partial pressure reaches a maximum at the end of inspiration, at half the respiratory cycle. The general behavior of the distribution in space of the partial pressure is reminiscent of the recent results of Swan and Tawhai (2011), in that there is heterogeneity of the pressure due to diffusion screening (if the diffusion coefficient of oxygen in air would be infinite, the pressure would be uniform). This heterogeneity is moderate in both cases because the surface permeability *although implemented in different manners*, is smaller than the usual membrane permeability $W = 72$ μm/s (see below).

The distribution in space and time of the oxygen flow is shown in Fig. 5. In the tree structure the surface approximately doubles at each generation. That explains why the deeper acinar regions dominate the transfer of oxygen and also displays a marked variation during the respiratory cycle.

We have performed the same calculations in the more complex case of an asymmetric acinus as described by Haefeli-Bleuer and Weibel (1988), see Appendix C. Assigning the experimental values for oxygen partial pressure and oxygen flow in this more complex geometry, one obtains $\Omega$ values ranging from 3.0 μm/s to 3.5 μm/s. There is however a difference between our results and the results of

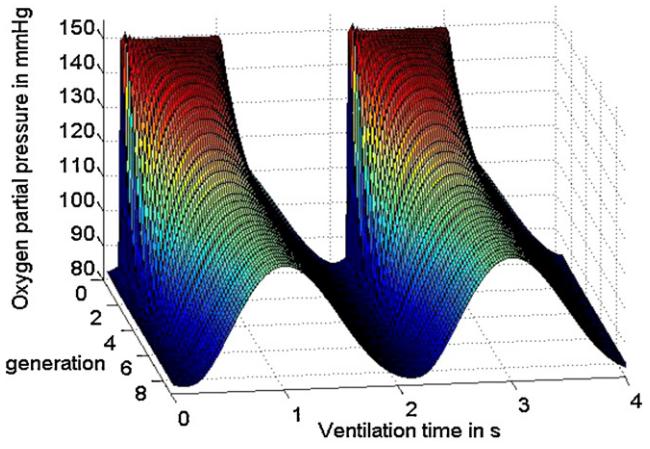


**Fig. 4.** Spatio-temporal distribution of the local partial pressure of oxygen $P(x,t)$, as a function of the generation (the integrative permeability $\Omega$ is taken equal to 3.5 μm/s). The time $t = 0$ corresponds to the beginning of inspiration. Note that the pressure increases to reach the value $PI_{O_2}$ only after a delay corresponding to the time of flight of air from the mouth to the acinus entrance (located at the rear of the figure).

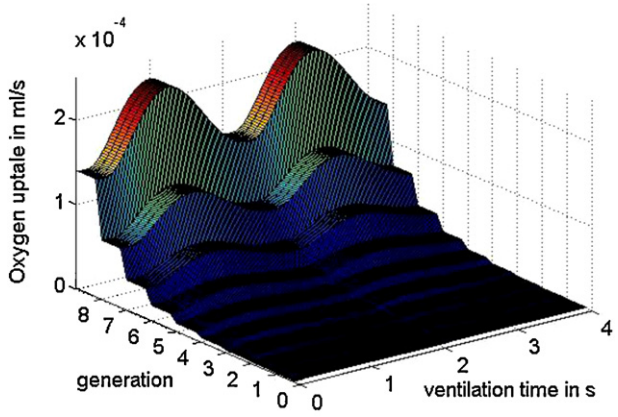


**Fig. 5.** Spatio-temporal distribution of the oxygen uptake. The acinus entrance is located at the front of the figure.

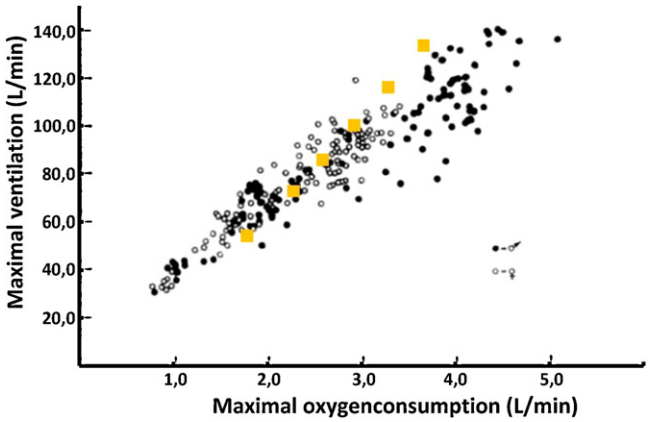


**Fig. 6.** Relation between the maximum oxygen flux (horizontal axis) and the ventilation at extreme exercise for various individuals and genders (vertical axis). From Astrand et al. (2003, p. 162). The yellow squares represent the results of our computation keeping the value of the integrative permeability equal to 3.5 μm/s.

Swan and Tawhai (2011) in the sense that here, an asymmetric acinus behaves not very differently from the symmetric case. We have no explanation for this difference, but it may come from a different splitting of the convective flux between the daughter branches in the two approaches. We recall that in the present approach, *the branches are themselves the pumps* that drive the convection.

Also, in the real lung, there exists a distribution of acini sizes. We have computed $\dot{V}_{O_2,max}$ and $PA_{O_2}$ in acini of different sizes. The results (Foucquier, 2010), not shown here, indicate that the flow at exercise is roughly proportional to the acinus volume. This is due to the fact that a larger acinus acts as a stronger pump. In consequence, the global oxygen uptake in a lung of a given volume is essentially independent of the size distribution of the acini. The net result of these computations is that, to account for experimental values of $\dot{V}_{O_2,max}$ and $PA_{O_2}$, the global transfer must be estimated by a value of the integrative permeability close to 3.5 μm/s or equivalently, 0.0046 μm/s/mmHg. This value is about four times smaller than the usually accepted value that is discussed below.

### 3.2. Athletes acini work like the machine acinus

Experimentally, Astrand et al. (2003) have shown that the oxygen consumption is a function of the ventilation and that there exist differences among individuals and between genders. These authors give measured ventilation and oxygen consumption in strong exercise for athletes of both genders. Reversing our point of view, we can now compute the oxygen consumption as a function of ventilation assuming a value $\Omega = 3.5$ μm/s. The results displayed in Fig. 6 (yellow squares) show a good agreement between the model and the experimental values at peak exercise. The fact that the many experimental values are found slightly below the yellow squares alignment can be attributed to alveolo-capillar partial pressure difference that may appear at extreme exercise.

The conclusion is that, at peak exercise, athletes acini work quantitatively like our machine acinus. This indirectly supports that the concept of integrative permeability can really account for blood saturation.

### 3.3. Comparison with the classic physiological description of the gas-capture process

In the usual language of physiology, the overall oxygen flow rate in the lung is usually described, after C. Bohr, as

$$\Phi = DL_{O_2} \times (PA_{O_2} - Pc_{O_2}) \tag{11}$$

where $DL_{O_2}$ is the "pulmonary diffusing capacity" (expressed in ml min$^{-1}$ mmHg$^{-1}$), $PA_{O_2}$ is the so-called "alveolar gas" partial pressure of $O_2$ supposed to be uniform (or averaged over gas space), and $Pc_{O_2}$ is the so-called oxygen partial pressure in capillary blood averaged (a) along the capillary path from the venous blood in the pulmonary arteriole to the venule that drains arterialized blood, and (b) over the entire capillary system of the lung.

Since Roughton and Forster (1957), the lung diffusive capacity is considered to be the result of two resistances in series measuring respectively diffusion and trapping. First $D_M$ measures the conductance of the diffusion barrier from the alveolar surface to the erythrocyte membrane, i.e. including the tissue barrier and the plasma layer (Weibel et al., 1993). Second $D_e$ measures the conductance of the complex processes within the erythrocytes comprising diffusion and chemical reaction. The Roughton and Forster decomposition writes:

$$DL_{O_2}^{-1} = D_M^{-1} + D_e^{-1} \tag{12}$$

Considerable efforts have been devoted to compute these two components from the morphometry of the capillary system for $D_M$ and from the chemical processes involved in hemoglobin trapping for $D_e$. The data determining $D_M$ and $D_e$ have been reviewed and discussed in (Weibel, 1984; Vock and Weibel, 1993; Weibel et al., 1993). One usually writes

$$D_M = \frac{K(SA_{lung} + Sc_{lung})}{2\tau_{hb}} = \frac{KSAc_{lung}}{\tau_{hb}} = W_M \times SAc_{lung} \tag{13}$$

where $K$ is the Krogh's diffusion coefficient, $SA_{lung}$ and $Sc_{lung}$ are the total alveolar and capillary gas exchange surfaces, respectively, their average being defined as an effective exchange surface $SAc_{lung}$. The quantity $\tau_{hb}$ is the harmonic mean thickness of the diffusion barrier (tissue and plasma taken together). This introduces the membrane permeability $W_M = K\tau_{hb}^{-1}$. The morphometric data for estimating $W_M$ for the human lung have been obtained by Gehr et al. (1978) and Weibel et al. (1993). The Krogh diffusion coefficient for tissue and plasma is taken to be $K = 5.5 \times 10^{-10}$ cm$^2$/s mmHg$^{-1}$. The relevant data here is $\tau_{hb} = 1.1$ μm, from which one derives $W_M = 0.095$ μm/s mmHg$^{-1}$ or $W_M = 72$ μm/s in physical units.

The erythrocyte component of $DL_{O_2}$ is usually expressed as $D_e = \theta_{O_2} Vc$ where $\theta_{O_2}$ is the reaction rate of $O_2$ with whole blood and $V_c$ is the capillary volume. The estimate of the reaction rate $\theta_{O_2}$ depends on in vitro measurements of the rate of $O_2$ uptake by whole blood $k'_c$ (Yamaguchi et al., 1985; Holland et al., 1985), the initial saturation $S_{O_2}$, the temperature $T$, the $O_2$ solubility $\alpha$ and the hemoglobin concentration [Hb]:

$$\theta_{O_2} = k'_c \cdot f(T) \cdot (0.0587\alpha_{O_2}) \cdot (1 - S_{O_2}) \cdot 0.01333[Hb]$$

As $O_2$ loading increases along the capillary, $\theta_{O_2}$ changes. However, according to the Bohr integration (Karas et al., 1987), it is accepted to consider an average value of $\theta_{O_2}$ along the capillary pathway for the human lung $\theta_{O_2} = 1.5\,ml_{O_2}\,ml_{blood}^{-1}\,min^{-1}\,mmHg^{-1}$.

In the following we concentrate on the values of the permeability and we write Eq. (1) as

$$\Phi = W_{eq} SAc_{lung}(PA_{O_2} - Pc_{O_2}) \tag{14}$$

introducing an equivalent global permeability $W_{eq}$. In the frame of the Roughton and Forster decomposition one can write

$$W_{eq}^{-1} = W_M^{-1} + W_e^{-1} \tag{15}$$

with $W_M = 72\,\mu m/s$ and $W_e = D_e/SAc_{lung} = \theta_{O_2} \cdot Vc/SAc_{lung}$.

Using $V_c = 194\,mL$ and taking $SAc_{lung} = 122\,m^2$ (Gehr et al., 1978; Weibel et al., 1993), one obtains $W_e = 0.040\,\mu m/s\,mmHg^{-1}$ and $W_{eq} = 0.022\,\mu m/s\,mmHg^{-1}$. Likewise, one obtains $DL_{O_2} = W_{eq} SAc_{lung} = 157\,mL\,min^{-1}\,mmHg^{-1}$.

In summary the usual physiological approach predicts $W_{eq} = 0.022\,\mu m/s\,mmHg^{-1}$ or $16\,\mu m/s$ in physical units.

### 3.4. Resolving or not the differences between the integrative permeability and the physiological approach

#### 3.4.1. Relation between the integrative permeability and the "true" permeability

By definition, the "true" permeability $W$ is the transport coefficient that would produce a flow $\Phi$ across the unit surface when a *constant* concentration difference $(C_1 - C_2)$ is applied between both sides of the surface

$$W = \frac{\Phi}{(C_1 - C_2)} \tag{16}$$

As stated before, the integrative permeability $\Omega$ plays the role of a calibration constant because it is determined by fitting the simulation results with the measured values of the oxygen flux. Its value then takes into account the effect of progressive blood saturation in which $(C_1 - C_2)$ is not constant (see for instance Scheid and Piiper, 1989). In blood, $P_{O_2}$ steadily increases as blood traverses the capillary network and become equilibrated with the *local* alveolar $PA_{O_2}$ before being discharged into the pulmonary veins with $Pa_{O_2}$. Linking $\Omega$ to $W$ requires a hypothesis on the progressive saturation along the capillary. At peak exercise, one can postulate that, in first approximation, the $P_{O_2}$ in capillary blood linearly increases from $Pv_{O_2}$ to $PA_{O_2}$ along the capillary length. In such a situation one would have $W \approx 2\Omega = 7.0\,\mu m/s$. The factor 2 is a *minimum* value that is obtained for a full use of the capillary network to achieve saturation, a reasonable hypothesis at extreme exercise. For an exponential saturation (Scheid and Piiper, 1989) with a time constant equal to $1/W$, the factor 2 would correspond to a 13% shunt effect. There exists then a difference between the usual physiological value $W_{eq} = 16\,\mu m/s$ and the value $W \approx 2\,\Omega = 7.0\,\mu m/s$ derived from the present analysis. Hereafter we discuss the causes for this discrepancy.

Of course, this is a simplified and idealized picture of respiration of athletes at peak exercise in the sense that perfusion is supposed to perfectly match oxygen trapping with a unique time constant, even though transit times are known to be distributed (Hogg et al., 1994; Presson et al., 1994).

The basic question to discuss is how blood equilibrates in time. This has been the subject of an immense literature. In the following, we do not solve the problem, but we recall a few basic concepts that lead to the idea that the purely diffusive component has been significantly overestimated in the morphometric approach.

#### 3.4.2. Dynamics of the blood oxygen equilibration process: the Roughton and Forster mechanism in the time domain

The trapping of oxygen by blood cells occurs through several successive steps, namely:

1- Alveolar oxygen has to be dissolved at the interface between the gas and the membrane considered to be essentially made of water.
2- The dissolved oxygen has to diffuse across the membrane and the plasma layer to reach the surface of the erythrocytes.
3- Oxygen is exchanged across the thin RBC membrane.
4- Oxygen diffuses across a very thin plasma layer to reach the first hemoglobin molecules.
5- Finally, oxygen has to be trapped by the hemoglobin molecules.

Each of these steps occurs over different time durations, which makes essential the distinction between on the one hand, extremely rapid, "local" processes across interfaces and on the other hand, macroscopic diffusion speed and capture which finally govern equilibration.

Let us first recall the nature of the dynamical process that leads to the oxygen equilibrium between different phases usually described by their solubility. Solubility is often measured in mol per mmHg, but we prefer here to express it through the equivalent "Oswald partition ratio". The partition ratio of a species $A$, here oxygen, between a gas and a liquid is the *dimensionless* ratio $\alpha$ of the concentration of $A$ in the liquid $C_L$ to concentration $C_g$ in the gas:

$$\alpha = \frac{C_L}{C_g} \tag{17}$$

In a kinetic description of thermal equilibrium between phases, the value of the partition ratio results from the equilibration between the flux of oxygen being trapped by the liquid, and the flux escaping it. If we call $W_{g\to L}$ and $W_{L\to g}$ the respective rates (probability per unit time) for a molecule to be trapped or to escape the liquid, equilibrium is reached when

$$C_L W_{g\to L} = C_g W_{L\to g} \tag{18}$$

which means that the partition coefficient $\alpha = C_L/C_g$ can be written as

$$\frac{C_L}{C_g} = \alpha = \frac{W_{g\to L}}{W_{L\to g}} \tag{19}$$

Eq. (19) represents the equality between the partial pressures on both sides of the interface. The fact that this oxygen partition ratio is of order of $2.4 \times 10^{-2}$ for water means that the probability for an oxygen molecule to leave the liquid is around $1/(2.4 \times 10^{-2}) = 42$ times larger than the probability for an oxygen molecule in the gas to be trapped by the liquid. But trapping or escape of oxygen is a molecular process with characteristic times of the order of 1–10 ps. Therefore, the concentration *in* the membrane *at* the alveolar membrane interface can be considered as instantaneously equilibrated according to the partition ratio.

The second step listed above is oxygen diffusion from the inner surface of the alveolar membrane toward the surface of red blood cells. A standard result for the diffusion across a *parallel* layer of thickness $\delta$ is the flux across the unit surface: $\Phi_M = C_g \alpha D_{O_2,H_2O}/\delta$. The quantity $W = \alpha D_{O_2,H_2O}$ is the Krogh's diffusion coefficient (note that $\alpha D_{O_2,H_2O}$ should not be called diffusivity, as it does not describe the diffusion inside a *single* medium).

Now, one should consider *two different times*. First, the time $T_D$ for a diffusing particle to cross a distance $\delta$ *in a homogeneous media* is of the order $T_D = \delta^2/D_{O_2,H_2O}$. With $\delta$ of order 1 micron and $D_{O_2,H_2O} = 30 \times 10^{-6}\,cm^2/s$, $T_D$ is of order 0.3 ms, much shorter than the time spent by the blood inside the capillaries. However the time to diffuse on a length $\delta$ of order 1 micron *from the gas* is

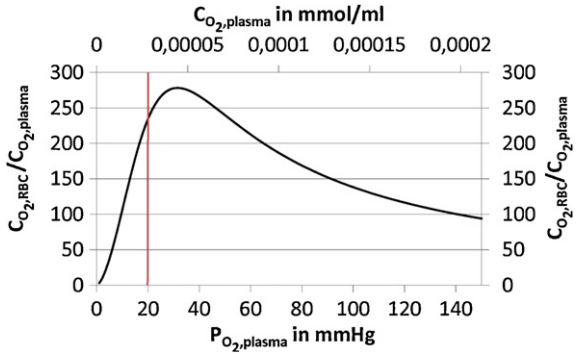


**Fig. 7.** Oxygen partition ratio as a function of the oxygen partial pressure in the plasma.

$\delta/W = T_D/\alpha$ of order 12 ms (the process is slowed down by the large escape probability).

Note that the description of the dynamical process above indicates that the role of plasma recirculation is negligible in transporting oxygen because the recirculation times should be compared with the ordinary diffusion time of order 0.3 ms. This is due to the fact that recirculation does not affect the molecular layer in the membrane from which oxygen tends to escape into the alveolar gas.

At the interface between the plasma and the red blood cell, the molecular process, step 3, is again very rapid. But now oxygen is much more "soluble" in the red blood cell than in the plasma. The correct local boundary condition at the interface between plasma and the interior of the cell should be written as $C_{RBC,i}/C_{plasma} = \alpha'$, where $\alpha'$ is the partition ratio between plasma and RBC. It can be computed from the number of Hb molecule per cell, the number of oxygen sites per Hb molecule, the Hill saturation curve and the RBC volume. It is now a number much larger than 1. This means that, inside a blood cell, an oxygen molecule has very little probability of escaping to the plasma. Due to the non-linear character of the Hill curve, the partition ratio between plasma and RBC is also non-linear as shown in Fig. 7. Note that the product $\alpha\alpha'$ is of order 3 (for arterial blood) in agreement with the known fact that the oxygen content of 1 l of blood and 1 l of air are close for an hematocrit of 40%.

The next step, 4 as listed above, corresponds to the diffusion time to reach Hb molecules. It is of order of $(r_{RBC})^2/D_{RBC}$ where $r_{RBC}$ is of order the radius of the cell (around 3 μm) and $D_{RBC}$ the diffusion coefficient of oxygen inside the RBC, of order $10^{-5}$ cm$^2$/s. One obtains a duration around 10 ms, again smaller than the time spent by the blood within the capillaries.

Finally, for step 5, one should take into account the finite reaction speed of oxygen with hemoglobin but the experimental values are at most of order 20 ms for the slowest process (Yamaguchi et al., 1985). In summary, the time required to transfer oxygen from alveolar gas to hemoglobin could be of order 50 ms, again a time shorter than the time spent by blood in the capillaries.

It is interesting to note that, because oxygen is much more soluble in RBC than in plasma, as soon as oxygen molecules reach the RBC surface they are trapped there so that the concentration in the plasma near a cell is maintained close to 0 (or more precisely to the concentration of oxygen in the venous plasma). This fact should last during a significant fraction of the equilibration time.

But perhaps the most important result of the above discussion is the general fact that, *during the beginning of equilibration*, the time scale is $\delta/v = \delta/W_M$. If the accepted values $\tau_{hb} = 1.1$ μm and $W_M = 72$ μm/s mentioned above are correct, the slope in time of blood saturation should start with a slope equal to 1.1/72 = 15 ms. There is then a contradiction between the values deduced from the usual morphometric approach and the fact that blood is equilibrated in a much longer time, suggesting that the classical value of $W_M$ may be overestimated.

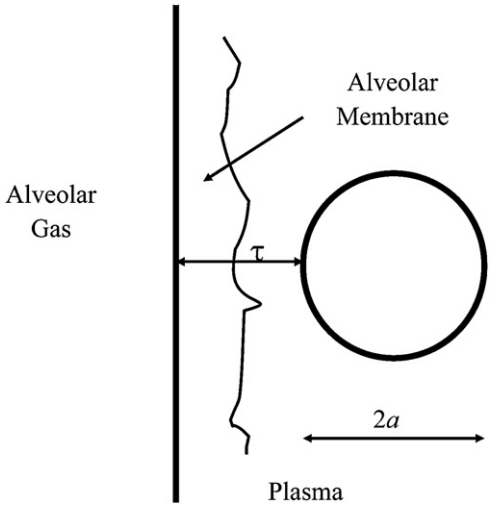


**Fig. 8.** Schematic of the computation of the diffusive flux between a flat interface and a spherical blood cell.

At this point we are faced with the question of why the diffusive permeability should be smaller than usually considered. To enter this question we first discuss a case study for which exact results can be drawn from existing literature.

*3.4.3. A case study: transfer from a flat alveolar space toward a "spherical blood cell". Toward a bottom-up approach to the value of the diffusive permeability?*

The value of the purely diffusive component of the lung diffusing capacity has been the subject of many studies (Federspiel, 1989; Weibel et al., 1993; Franck et al., 1997; Hsia et al., 1995, 1997 and the references therein). The problem is to solve the steady-state diffusion equation $\Delta C = 0$ (Laplace equation) with boundary conditions $C = 1$ on the diffusion source, and $C = 0$ on the blood cell surfaces. The above authors have used finite element methods calculations to evaluate the diffusive capacity of spherical and parachute shaped RBC cells in cylindrical capillaries.

There is however an enlightening case on which we wish to attract attention. It is the case of a planar membrane and a spherical RBC of radius $a$ at distance $\tau$ (Fig. 10). Indeed, Maxwell (1873) gave an exact solution for an exactly equivalent Laplacian problem, the capacitance of a capacitor with a planar electrode and a sphere of radius $a$ at distance $\tau$ (Fig. 8):

$$C = 4\pi\varepsilon_0 a F(a/\tau) \quad \text{with} \quad F(a/\tau) = \sum_{n=1}^{+\infty} \frac{\sinh(\ln A)}{\sinh(n \ln A)} \quad \text{and}$$

$$A = 1 + \frac{\tau}{a} + \left[\left(1 + \frac{\tau}{a}\right)^2 - 1\right]^{1/2} \tag{20}$$

The corresponding solution for the diffusing capacity between a planar membrane and a spherical blood cell is then, assuming that oxygen diffusivities are the same in the membrane and the plasma, and replacing $\varepsilon_0$ by $\alpha D_{O_2}$:

$$D_{cell} = 4\pi a \alpha D_{O_2,H_2O} F(a/\tau) \tag{21}$$

Eq. (22) is complicated, but, when the distance $\tau$ is much smaller than the radius $a$, one can show that $F(a/\tau)$ behaves as a linear

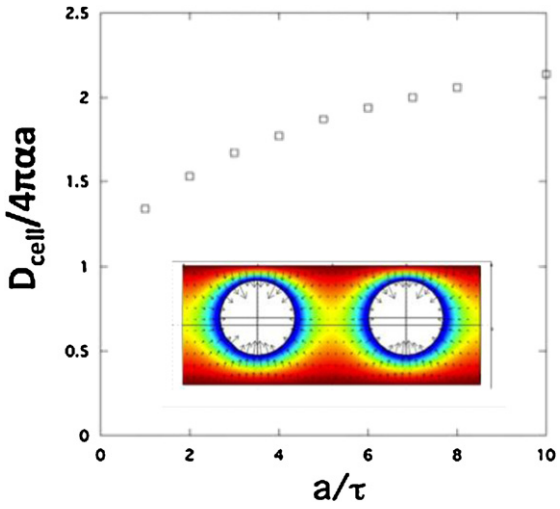


**Fig. 9.** Dependence of the diffusive capacity toward a spherical blood cell. One observes that a factor 10 in the distance modifies the diffusive value only by a factor 40%. The inset picture, obtained through 3D FEM calculation, displays the concentration map coded in color from 1 (dark red) to 0 (dark blue). The figure illustrates the fact that the entire surface of the blood cell is used for transfer as the local flux on the surface is approximately proportional to the inverse of the thickness of the dark blue layer.

function of $\ln(a/\tau)$. Thus the diffusivity of a single spherical cell *depends very slowly on the distance between the cell and the planar source* (Crowley, 2008). This is illustrated in Fig. 9 in which one observes also that the value of $F(a/\tau)$ is of order 1. So, in a first approximation, the value $D_{cell,\infty} = 4\pi a\alpha D_{O_2,H_2O}$ (for $\tau$ infinite) is a "universal" order of magnitude. Note that, if one wishes to recover the usual dimensional formulation of a diffusive capacity, surface divided by distance, one could attribute a surface of the order of the surface of the half sphere: $S = 2\pi a^2$, and a "mean" distance of order $\tau = a/2$, so that the conductance would be $D_{cell} = \alpha D_{O_2,H_2O}(S/\tau) = \alpha_{O_2} D_{O_2,H_2O}(2\pi a^2)/(a/2)$ or again $4\pi a\alpha_{O_2} D_{O_2,H_2O}$.

The most significant qualitative conclusion of this example is that the very slow dependence of the flow on the distance to the wall implies that a large fraction of the surface is used for transfer. This is illustrated in the inset of Fig. 9 which displays a color map of the spatial distribution of the concentration of oxygen around a spherical blood cell maintained at zero concentration and placed between two parallel membranes. This is the result of 3D finite elements calculation of steady-state diffusion. One observes that the flux near the surface, proportional to the inverse thickness of the dark blue layer (local gradient) around the sphere, varies only slowly around the surface perimeter. The value of this cell diffusive capacity is $D_{cell,\infty} = 1.42 \times 10^{-9}$ cm$^3$ s$^{-1}$ for a = 2.7 μm. Note that this value corresponds to a single membrane.

This is to be compared to previous results in the literature:

- Federspiel (1989) has used FEM to compute RBC $D_{MO_2}$ in capillaries in various circumstances (distance, hematocrit, etc.). For diluted RBC (small hematocrit) he found a value $D_{M,RBC} = 2 \times 10^{-9}$ cm$^3$ s$^{-1}$ compared to be compared to $2 \times D_{cell,\infty} = 2.84 \times 10^{-9}$ cm$^{-1}$ s$^{-1}$.
- Hsia et al. (1995) used FEM to compute RBC $D_{MCO}$ in capillaries in various circumstances (distance, hematocrit, etc.) for parachute shaped RBC but using the Roughton and Forster decomposition to take care of Hb saturarion. Correcting for solubility and diffusivity their result is $D_{M,RBC} = 1.2 \times 10^{-9}$ cm$^{-1}$ s$^{-1}$.
- Franck et al. (1997) also used FEM to compute RBC $DM_{O_2}$ in capillaries in various circumstances (distance, hematocrit, etc.) for parachute shaped RBC. For diluted RBC (small hematocrit) they obtain a value $D_{M,RBC} = 3.3 \times 10^{-9}$ cm$^3$ s$^{-1}$ of the same order.

Note that a value of $10^{-9}$ cm$^3$ s$^{-1}$ would correspond to a time constant to fill a RBC volume (90 μm$^3$) equal to 0.9 s, which is of the right order of magnitude if saturation is obtained in 2 or 3 time constants.

It is beyond the scope of the present work to discuss the reasons for the differences between these results, computed in somewhat different circumstances, but it is of interest to note that they resulted in the same order of magnitude. These authors also mention that *a large fraction of the surface is used for transfer.* This is also observed in Fig. 10 for biconcave RBC. One observes that the local flux is large at top and bottom of the cells, and reaches a *small* surface, in contrast with the smaller flux on the *larger* lateral surfaces. There is however a (small) difference between the diffusing capacities of a biconcave blood cell and that of a spherical cell of the same volume. We write the diffusive capacity of a single biconcave cell as

$$D_{cell} = 4\pi a\alpha D_{O_2,H_2O} F(a/\tau)\Sigma(\tau) \quad (22)$$

where we have added a shape factor $\Sigma(\tau)$ that weakly depends on the distance $\tau$. The comparison of the flow computed for a biconcave cell and a spherical cell gives, respectively $\sum(\tau) = 0.70$, 0.74, 0.76 for $\tau = 0.5$, 1, 1.5 μm. Of course, the alveolar surface itself is not flat but as the diffusive flux reaches a large fraction of the erythrocyte surface this should not modify significantly the value of the permeability.

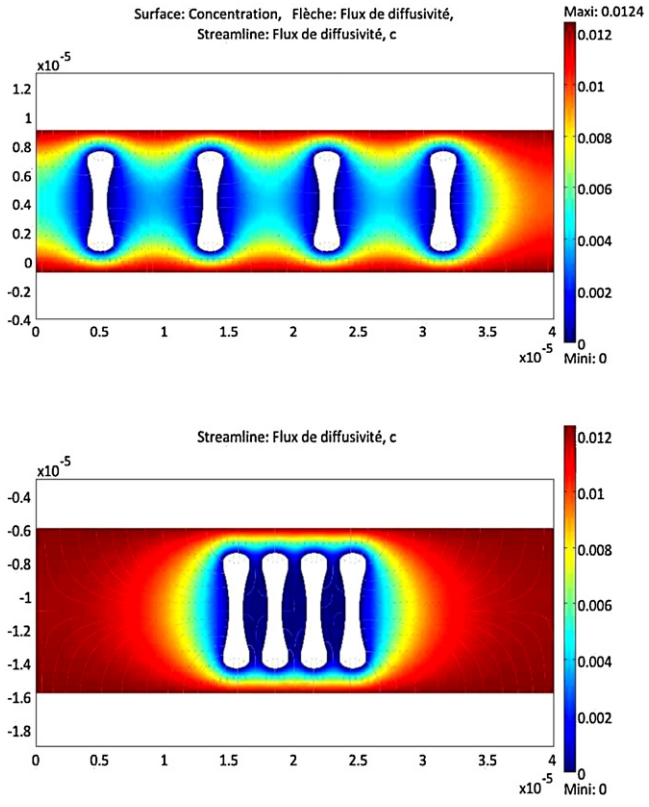


**Fig. 10.** Color map of the oxygen concentration around biconcave blood cells. Top: diluted cells corresponding to small hematocrit. One observes that the local flux (proportional to the inverse thickness of the dark blue layer) is less uniformly distributed than in the case of a sphere in the inset of Fig. 9. Bottom, when the cells are more concentrated, which corresponds to large hematocrit or to clusters, the lateral surfaces between narrowly spaced cells are inactive.

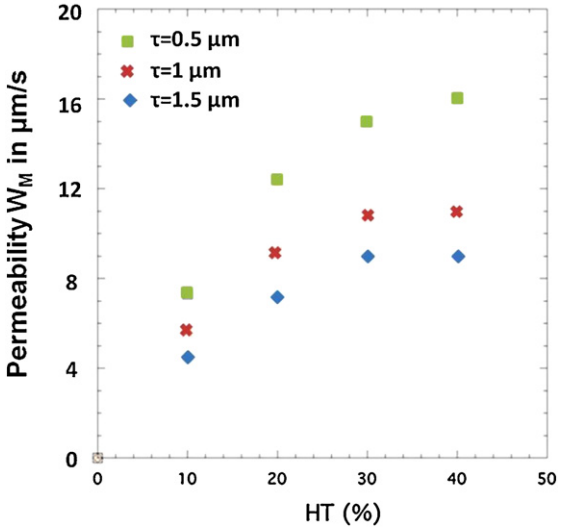


**Fig. 11.** Global diffusive permeability as a function of the hematocrit for equally spaced biconcave blood cells. Square, crosses and diamonds respectively correspond to $t = 0.5$, 1, and 1.5 μm. One observes a saturation effect for large hematocrit which is due to the screening of diffusion fluxes illustrated in Fig. 10, bottom.

*3.4.4. From one blood cell to the value of the permeability*

If there are on average $N_{RBC}$ red blood cells par alveolar unit surface, the permeability is equal to

$$W = 4\pi a \alpha D_{O_2,H_2O} N_{RBC} F(a/\tau)\Sigma(\tau) \quad (23)$$

*if* the permeability is simply *proportional* to the number of red blood cells. We now evaluate the number of RBC in front of a unit surface (1 $cm^2$) using the values admitted in the literature. There are 180 $cm^3$ of blood in front of a surface of order 130/2 $m^2$ which amounts to $2.8 \times 10^{-4}$ $cm^3$ of blood per $cm^2$ of alveolar surface. The volume of a blood cell is of the order of 100 $\mu m^3$. It would then be possible to pack $2.8 \times 10^6$ RBC in front of 1 $cm^2$ if the hematocrit *Ht*, or packed cell volume (PCV), or erythrocyte volume fraction (EVF), would be 100%. It is normally about 48% for men and 38% for women, but some authors have given a value of hematocrit in the capillaries around 20% so that $N_{RBC}$ would be of on the order of $5.6 \times 10^5$ (McWhirter et al., 2009).

Following Eq. (23), large values of the hematocrit would increase the permeability *if diffusive flux toward the blood is proportional to it*. There are results in the literature (Federspiel, 1989; Franck et al., 1997; Hsia et al., 1995, 1997) showing that when *Ht* is of order 30–40%, screening effects appear and reduce the flux per cell in agreement with the flux as illustrated in the bottom panel of Fig. 10.

The dependence of permeability on the hematocrit based on our FEM calculations of the flux for bi-concave cells is shown in Fig. 11 for three values of the distance $\tau = 0.5$, 1, and 1.5 μm. For the three values of $\tau$, the permeability is strongly non-linear and one observes a saturation of the permeability; for example for $\tau = 1$ μm, $W = 10.5$ μm/s for about HT > 30%.

It is striking that the purely diffusive resistance under the extreme circumstance where *RBC internal diffusion and trapping by Hb are infinitely fast* may be one order of magnitude smaller than what was considered before. The fact that the diffusive resistance might be larger than that considered in the morphometric approach has already been discussed in several publications (Franck et al., 1997; Fung, 1997; Albrecht et al., 1979; Watson et al., 1987; Hsia et al., 1995, 1999; Hsia, 2002; Tamhane et al., 2001).

If now, in a conservative Roughton and Forster approach, we compute the global permeability by combining the inverse permeabilities as in Eq. (15), we obtain: $W_{eq} = 7.8$ μm/s. The time to reach the hemoglobin molecules at a distance of order $\delta = 2$ μm is of the order of 0.25 s, close to the time spend by blood to flow through capillaries at extreme exercise.

In addition, if the hematocrit is too large, blood cells can aggregate and build clusters (Zavorsky et al., 2004; Calbet et al., 2008; McWhirter et al., 2009). This phenomenon has been observed in many recent micrographs of capillaries and recent hydrodynamics studies of blood cells, considered as vesicles. In that situation, part of the cell surface will be lost for oxygen transfer. Note also that the real value of the hematocrit inside the capillaries during respiration is not experimentally accessible.

The evaluation of *W* given above accounts, although in a different manner, for the dependence of the lung diffusive capacity on $V_c$ (capillary volume): the larger $V_c$ the larger the number of blood cells $N_{RBC}$ adjacent to the alveolar membrane, and the larger the *purely diffusive* permeability.

*3.4.5. Implications of our results and relation to experiment*

One should note that, in the description of the functioning of the machine acinus, there is no need to consider the concept of the diffusing capacity $DL_{O_2}$. The question arises only when one wishes to use the notion of a capillary pressure (that cannot be measured directly) to relate the integrative permeability to the true permeability, also a quantity that cannot be measured experimentally.

This last question however disappears in the case of the diffusing capacity of NO: $DL_{NO}$ (Guénard et al., 1987). In the case of NO the affinity for hemoglobin is so large that the hemoglobin resistance (second term in the Roughton and Forster formulation) can be neglected so that $DL_{NO} = DM_{NO}$. This quantity has been measured (Zavorsky and Murias, 2006) and the experimental value of $DM_{NO}$ yields an estimated value for $DM_{O_2}$ around 9 μm/s, after adaptation to account for the change in solubility and diffusivity. What is important here is that, contrary to oxygen, the (Zavorsky and Murias, 2006) experiments are single breath *in which there is no dynamical screening*. This is close to the value 10.5 μm/s mentioned above. This may be considered direct evidence that the diffusion term for oxygen is a factor 7 smaller than that deduced from the usual morphometric approach (it is possible that the difference between the value 10.5 μm/s deduced from our approach and the value 9 μm/s deduced from Zavorsky is due to a possible resistance to NO transfer of the red cell membrane). This fact has been discussed recently (Borland Colin et al., 2010), but we cannot make a conclusion on this issue because the analysis in this paper was performed using the Roughton and Forster decomposition.

## 4. Summary and discussion

In this work, we have computed the gas exchange dynamics in a breathing machine acinus under the condition that it reproduces the measured physiological requirements, namely the value of the oxygen flux and the averaged alveolar pressure that allow for blood equilibration. The most relevant result of our work is that, even for the simplified functioning of this machine acinus, the oxygen flux is *not* proportional to the permeability as formerly suggested by the Bohr expression. This is due to the complex behavior of the dynamics of the diffusion–convection–permeation flow during the respiratory cycle.

The oxygen partial pressure in the alveolar space was found to be heterogeneously distributed in space and time. This could modify the evaluation of saturation as the partial pressure is found to drop below 100 mmHg during a significant fraction of the cycle.

Our calculations gives a quantitative prediction of the dependence of the oxygen consumption on vital capacity in good agreement with experiments for athletes at peak exercise.

The factor that governs the dynamics of the acinus functioning is the value of the permeability. Only a narrow range of permeability values is compatible with $DM_{O_2}$ values that allows for blood saturation. There is, however, a discrepancy of order 2 between the value of the permeability that is required to justify both $\dot{V}_{O_2,max}$ and $PA_{O_2}$ and the classic value in the literature. This is the necessary conclusion from the top to bottom study of oxygen exchange.

In a bottom-up approach to the computation of this diffusive permeability, we have given a new formulation based on totally different inputs, namely the size of the red blood cells and the hematocrit, plus correction factors of order 1 that depend on the RBC shape and distance to the alveolar space. The conclusion of this new approach is that the usual way to compute the diffusive part of the permeability using the harmonic mean of the distance between the alveolar space and blood cells leads to an overestimation of this diffusive component.

A striking result is that the permeability values, on the one hand deduced from the top to bottom calculation of the dynamics of the respiratory cycle, on the other hand deduced from our bottom-up approach, are very similar and that they also are in good agreement with the ones deduced from $DL_{NO}$ measurements.

Of course, each of these independent facts could be criticized in the sense that they rely on various different parameters that cannot be really known perfectly, but the general agreements lends confidence to both calculations. The net result is that the permeability is smaller that usually accepted and this is due to the fact that its diffusive component was previously significantly overestimated.

More generally, the qualitative but general conclusion presented leads one to re-examine several aspects of the common understanding of respiration:

1 The dynamics of respiration play an essential role. The system response is not a linear function of the usual parameters, like the permeability for example, and it is not clear at this stage how one should define the functioning of an equivalent steady state system that could be described by a Bohr type of formulation.
2 The steady state Bohr approach that is aimed at describing an average of the respiratory cycle should be re-examined on several points. First, it formulates the oxygen flux as a function of an alveolar and capillary pressure that cannot be measured. Second, blood is a complex fluid made of two components, plasma and erythrocytes that are not in chemical equilibrium during oxygen capture. Because these components are not in equilibrium there does not exist, even locally, a "blood oxygen partial pressure". This is shown in Fig. 10 displaying the spatial variation of the oxygen concentration in the capillary. A single blood oxygen partial pressure does exist in the venous and arterial blood, because both components, plasma and RBC, are equilibrated, but not during gas exchange.
3 In the same spirit the notion of the "lung diffusive capacity" may be dubious because it links a quantity that can be measured, the oxygen flow, to an ill-defined "capillary pressure" and to averaged partial pressures that cannot be measured.
4 The Roughton and Forster formulation, in the sense that it proposes an interpretation in terms of a "steady state" respiration picture should also be re-examined. Though this may appear a bold assumption, our approach qualitatively suggests that experiments interpreted through the Roughton and Forster model could give inconsistent results. The present work implies that the blood hematocrit percentage plays a role not only in $D_e$ but also directly in $D_M$.
5 Furthermore, the Roughton and Forster decomposition supposes that the surfaces of the blood cells remain at the same concentration during oxygen transfer. But this has no real justification as suggested by the case of the spherical cell: if the overall diffusion currents reach a large fraction of the cell surface, *there must be a distribution of diffusion paths* that reach the cell. Between them, some are short (and rapid) and reach a small fraction of the surface while the majority is longer (and thus slower) and reach a larger fraction of the surface, making the real dynamics more complex than implied by the Roughton and Forster model. On the other hand, as stated above, the diffusion inside the erythrocyte is rapid, with a tendency to equalize the oxygen partial pressure in the interior of the RBC. Future studies of the *complete time dependence* of the diffusion process with the trapping dynamics should be performed through numerical simulations. Similar calculations could be done for other gases of interest such as the example of NO discussed below.
6 In addition, during the time spent by erythrocytes in the capillaries, much of the system is moving and changing shape, in particular the RBCs shapes. The real situation is so complex that a realistic computation of the diffusive permeability is not feasible at this time. However, it seems a priori reasonable to use a single breath measurement of $DL_{NO}$ because the cyclic role of respiration does not play a role and the RBC could be modeled as a sink for NO (see however Vaughn et al., 2000; Borland Colin et al., 2010). *In particular the difference between rapid and slow diffusion paths should play no role for* NO *because a single breath measurement is essentially a steady state experime*nt. The agreement mentioned above between the $W_M$ values deduced from the bottom-up approach of the diffusive permeability, and the value deduced from $DL_{NO}$ measurements *refers to a steady state regime.* Thus the extrapolation from $DL_{NO}$ to the $DM_{O_2}$ of Roughton and Forster could be difficult because the transfer and capture of oxygen is dynamic.
7 In respiration, besides anatomy and respiratory cycle, there exists only three quantities that can be really known, the oxygen partial pressure in air (that can depend on altitude), the venous partial pressure and the measured oxygen flow. We suggest that the Bohr equation should be replaced by

$$\Phi = DL'_{O_2} \cdot (PI_{O_2} - Pv_{O_2}).$$

This new lung diffusive capacity $DL'_2$ is of course a closed "black box" that contains all the respiration complexities but is now defined only from measurable quantities. We believe that the opening of this new black box should result from numerical studies of *the dynamics of the complete saturation process for the various gas of interest*, $O_2$, CO, and NO. From our point of view, it is far from clear that *the results of the dynamics* could be accurately expressed as *two steady state resistances in series*. This should be the object of future work.
8 The same methodology can be applied to the study of the respiration at rest where the situation is more complex. Several possible factors have to be considered: reduced cardiac output, different venous oxygen saturation and possible hypoxic vasoconstriction in the regions with small oxygen partial pressure. The study of the dynamical effects on respiration at rest will be published elsewhere.

## Acknowledgements

This work was started many years ago. During this period, we had more that a large number of discussions with Ewald Weibel. We are greatly indebted to him for the richness of these scientific exchanges. We wish also to thank Hervé Guénard for interesting

discussions and information on diffusion measurements and Sunita Darbe for a careful reading on the manuscript. Ira Katz is gratefully acknowledged for his many fruitful remarks on the text. The authors wish to thank the French agency ANR (project SAMOVAR, n°2010-BLAN-1119) for financial support.

## Appendix A. Numerical methods

The transport equations inside the acinus are discretized through a finite differences method:

- For a point inside a branch:


$$\frac{\partial J(x)}{\partial x} \rightarrow \frac{J_{i,i+1} - J_{i-1,i}}{\frac{h_{i,i+1} + h_{i-1,i}}{2}}$$

- For a bifurcation point:

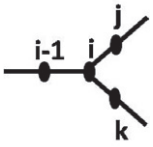


$$\frac{\partial J(x)}{\partial x} \rightarrow \frac{J_{i,j} + J_{i,k} - J_{i-1,i}}{\frac{h_{i,j} + h_{i,k} + h_{i-1,i}}{2}}$$

The time-dependent part of the equation is solved using a Crank–Nicholson scheme. For a point inside a branch, the discrete drift-diffusion equation therefore writes:

$$\frac{P_i^{t+\Delta t} - P_i^t}{\Delta t} = -\frac{WS_{Ac}}{V}\left(\frac{P_i^{t+\Delta t} + P_i^t}{2}\right) + \frac{WS_{Ac}}{V}P_{blood} - \frac{1}{2}\left(\frac{J_{i,i+1}^{t+\Delta t} - J_{i-1,i}^{t+\Delta t}}{(h_{i,i+1}^{t+\Delta t} + h_{i-1,i}^{t+\Delta t}/2)}\right) - \frac{1}{2}\left(\frac{J_{i,i+1}^{t} - J_{i-1,i}^{t}}{(h_{i,i+1}^{t} + h_{i-1,i}^{t}/2)}\right)$$

and for a bifurcation point:

$$\frac{P_i^{t+\Delta t} - P_i^t}{\Delta t} = -\frac{WS_{Ac}}{V}\left(\frac{P_i^{t+\Delta t} + P_i^t}{2}\right) + \frac{WS_{Ac}}{V}P_{blood} - \frac{1}{2}\left(\frac{J_{i,j}^{t+\Delta t} + J_{i,k}^{t+\Delta t} - J_{i-1,i}^{t+\Delta t}}{(h_{i,j}^{t+\Delta t} + h_{i,k}^{t+\Delta t} + h_{i-1,i}^{t+\Delta t}/2)}\right) - \frac{1}{2}\left(\frac{J_{i,i+1}^{t} + J_{i,k}^{t} - J_{i-1,i}^{t}}{(h_{i,i+1}^{t} + + h_{i,k}^{t} + h_{i-1,i}^{t}/2)}\right)$$

## Appendix B.

The time being discretized in small time steps $\Delta t$, the air velocity writes

$$U_i(t)A_i(t) = \frac{\Delta V_i}{\Delta t} \tag{B1}$$

where $A_i(t)$ is the hydrodynamic cross-section at time $t$ of the alveolar duct at site $i$ and $\Delta V_i$ is the change in acinar volume distal to the site $i$ during the time $\Delta t$. We use the hydrodynamic cross-section due to the presence of the alveoli along the ducts (Tsuda et al., 1995). This assumes the presence of a hydrodynamic flow inside a portion of each alveolus.

Measurements have shown that, in first approximation, only the ducts follow the alternating volume change during the respiratory cycle whereas the alveolar sleeve shows only small changes (Bachofen and Schürch, 2001). So the duct lengths and cross-sections including alveoli dilate as $k(t)$ and $k(t)^2$ where $k(t)$ is given by:

$$k(t) = \left[1 + \delta\left(\frac{1 - \cos(2\pi f t)}{2}\right)\right]^{1/3} \tag{B2}$$

The dilation of the alveolar surface during the respiratory cycle is significantly smaller than that of the external volume (Bachofen and Schürch, 2001). This is the reason why we assume, in first approximation, that the diameter of the alveolus is time-independent. So, the effective cross-section $A_i(t)$ depending on the hydrodynamic diameter writes

$$\begin{cases} A_i(t) = \frac{\pi}{4}\left[k(t)d_{out,i}(t=0) - \frac{3}{4}(d_{out,max,i} - d_{in,max,i})\right]^2 & \text{if } g < 3 \\ A_i(t) = \frac{\pi}{4}\left[k(t)d_{out,i}(t=0) - \frac{1}{2}(d_{out,max,i} - d_{in,max,i})\right]^2 & \text{if } g \geq 3 \end{cases} \tag{B3}$$

where $d_{out,i}(t=0)$ is the external diameter of the duct $i$ at the beginning of the cycle, $d_{out,max,i}$ is the external diameter at 100% TLC, and $d_{in,max,i}$ is the internal diameter at 100% TLC. These last two parameters are time-independent. The distinction between the cases $g<3$ and $g\geq 3$ comes from the fact that the ducts of the first three generations are just partially covered by alveoli (Haefeli-Bleuer and Weibel, 1988). Similarly, the volume $V_i(t)$ writes

$$V_{ducts,i}(t) = \frac{\pi}{4}k(t)\ell_i(t=0) \times \left[k(t)d_{out,i}(t=0) - (d_{out,max,i} - d_{in,max,i})\right]^2 \tag{B4}$$

The velocity is then deduced

$$\begin{cases} U_i(t) = \frac{(d/dt)[k(t)\ell_i(t=0)[k(t)d_{out,i}(t=0) - (d_{out,max,i} - d_{in,max,i})]^2]}{(k(t)d_{out,i}(t=0) - (3/4)(d_{out,max,i} - d_{in,max,i}))^2} & \text{if } g < 3 \\ U_i(t) = \frac{(d/dt)[k(t)\ell_i(t=0)[k(t)d_{out,i}(t=0) - (d_{out,max,i} - d_{in,max,i})]^2]}{(k(t)d_{out,i}(t=0) - (1/2)(d_{out,max,i} - d_{in,max,i}))^2} & \text{if } g \geq 3 \end{cases} \tag{B5}$$

## Appendix C. Role of the acinar asymmetry

The real acinar geometry consists of a branching tree including up to 11 generations with both topological and geometrical asymmetries. In our model, these two asymmetries are described using two types of parameters:

- The first parameter, called *interruption probability* and denoted $p$, accounts for the probability of terminating a pathway; at each new possible bifurcation, there is a probability $1-p$ of continuing a segment and $p$ of stopping it. In their complete description of several human acini, Haefeli-Bleuer and Weibel (1988) have shown that terminal ducts are found in the tree structure from the 7th generation onward. This topological asymmetry is modeled by imposing a generation-dependent value of this parameter $p$ in our model geometry: $p$ is very small at generations 7 and 8 and larger in generations 9 and 10.
- The second parameter corresponds to the relative standard deviation of the branch size and diameter distribution at each generation. The geometry of our model acinus is randomized using Gaussian distributions.

All these parameters are fitted to the detailed experimental data found in Haefeli-Bleuer and Weibel (1988). In this realistic

geometry, we consider that the average of the inner diameter is approximately constant equal to 0.5 mm from generation 0 to 2, due to the small number of alveoli. It abruptly decreases from 0.4 mm at the 3rd generation, where the alveoli become more abundant, to 0.25 mm at the 11th generation.

The detailed account of these computations is out of the scope of the present paper. It can be found in Foucquier (2010). The net results of the computation of the convection–diffusion–permeation equations in these more realistic acini are values of the integrative permeability comprised between $\Omega = 3.0\,\mu m/s$ and $\Omega = 3.5\,\mu m/s$.

## References


Albrecht, K.H., Gaehtgens, P., Pries, A., Heuser, M., 1979. The Fahraeus effect in narrow capillaries (i.d. 3.3 to 11.0 micron). Microvascular Research 78, 33–47.

Astrand, P.O., Rodahl, K., Dahl, H.A., Stromme, S.B., 2003. Treatise of Work Physiology, 4th ed. Human Kinetics, Champaign, IL, USA.

Bachofen, H., Schürch, S., Urbinelli, M., Weibel, E.R., 1987. Relations among alveolar surface tension, surface area, volume, and recoil pressure. Journal of Applied Physiology 62, 1878–1887.

Bachofen, H., Schürch, S., 2001. Alveolar surface forces and lung architecture. Comparative Biochemistry and Physiology A: Molecular and Integrative Physiology 129, 183–193.

Borland Colin, D.R., Dunningham, H., Botrill, F., Vuylesteke, A., Yilmaz, C., Merrils Dane, D., Hsia Connie, C.W., 2010. Significant blood resistance to nitric oxide transfer in the lung. Journal of Applied Physiology 108, 1052–1060.

Calbet, J.A.L., Robach, P., Lundby, C., Boushel, R., 2008. Is pulmonary gas exchange during exercise in hypoxia impaired with the increase of cardiac output. Applied Physiology, Nutrition, and Metabolism 33, 593–600.

Crowley, J.M., 2008. Simple expression for force and capacitance for a conductive sphere near a conductive wall. In: Proceedings of the ESA Annual Meeting on Electrostatics, p. Paper D1.

Dutrieue, B., Vanholsbeeck, F., Verbank, S., Paiva, M., 2000. A human acinar structure for simulation of realistic alveolar plateau slopes. Journal of Applied Physiology 89, 1859–1867.

Federspiel, W.J., 1989. Pulmonary diffusing capacity: implications of two-phase blood flow in capillaries. Respiration Physiology 77, 119–134.

Felici, M., Filoche, M., Sapoval, B., 2003. Diffusional screening in the human pulmonary acinus. Journal of Applied Physiology 94, 2010–2016.

Felici, M., Filoche, M., Sapoval, B., 2004. Renormalized random walk study of the efficiency of the mammalian pulmonary acinus. Physical Review Letters 92, 068101.

Felici, M., Filoche, M., Straus, C., Similovski, T., Sapoval, B., 2005. Diffusional screening in real 3D human acini – a theoretical study. Respiratory Physiology & Neurobiology 145, 279–293.

Filoche, M., Moreira, A.A., Andrade, J.S., Sapoval, B., 2008. Quantitative analysis of the oxygen transfer in the human acinus. Integration in Respiratory Control: From Genes to Systems 605, 167–172.

Florens, M., Sapoval, B., Filoche, M., 2011. An anatomical and functional model of the human tracheobronchila tree. Journal of Applied Physiology 110, 756–763.

Foucquier A., 2010. Dynamique du transport et du transfert de l'oxygène au sein de l'acinus pulmonaire humain. Thèse de Doctorat de l'Ecole polytechnique, pp. 108–121. Accessible on Pastel website: http://pastel.archives-ouvertes.fr/index.php?halsid=7ah4v9djubjgh1c9tvert860o5&action_todo=home (under the name Foucquier).

Franck, A.O., Chuong, C.J.C., Johnson Jr., R.L., 1997. A finie-element model of oxygen diffusion in the pulmonary capillaries. Journal of Applied Physiology 79, 2036–2044.

Fung, Y.C., 1997. Biomechanis: Circulation, 2th ed. Springer, New York.

Gehr, P., Bachofen, M., Weibel, E.R., 1978. The normal human lung: ultrastructure and morphometric estimation of diffusion capacity. Respiration Physiology 32, 121–140.

Grebenkov, D., Filoche, M., Sapoval, B., 2005. Diffusion–reaction in branched structures: theory and application to the lung. Physical Review Letters 94, 050602.

Guénard, H., Varène, N., Vaida, P., 1987. Determination of the lung capillary blood volume and membrane diffusing capacity in man by the measurements of NO and CO transfer. Respiratory Physiology 70, 113–120.

Haefeli-Bleuer, B., Weibel, E.R., 1988. Morphometry of the human pulmonary acinus. Anatomical Record 220, 401–414.

Hogg, C.H., Coxson, H.O., Breumwell, M.-L., Beyers, N., Doeaschuk, C.M., MacNee, W., Wiggs, B.R., 1994. Erythrocyte and polyùoronuclear cell transit time and cponcentration in human capillaries. Journal of Applied Physiology 79, 1795–1800.

Holland, R.A.H., Shibata, H., Scheid, P., Piiper, J., 1985. Kinetics of $O_2$ uptake and release by red cells in stopped-flow apparatus: effects of unstirred layer. Respiration Physiology 59, 71–91.

Hou, C., Gheorghiu, S., Huxley, V.H., Pfeifer, P., 2010. Reverse engineering of oxygen transport in the lung: adaptation to changing demands and resources through space-filling networks. PLoS Computational Biology 6, e1000902.

Hsia, C.C.W., Chuong, C.J.C., Johnson Jr., R.L., 1995. Critique of the conceptual basis of diffusing capacity estimates: a finite element method. Journal of Applied Physiology 79, 1039–1047.

Hsia, C.C.W., Chuong, C.J.C., Johnson Jr., R.L., 1997. Red cell distortion and conceptual basis of diffusing capacity estimates: a finite element method. Journal of Applied Physiology 83, 1397–1404.

Hsia, C.C.W., Johnson Jr., R.L., Shah, D., 1999. Red cell distribution and the recruitment of pulmonary diffusing capacity. Journal of Applied Physiology 86, 1460–1467.

Hsia, C.C.W., 2002. Recruitment of lung diffusing capacity: update of concept and application. Chest 122, 1774–1783.

Karas, R.H., Taylor, C.R., Jones, J.H., Linstedt, S.L., Reeves, R.B., Weibel, E.R., 1987. Adaptive variation in the mammalian respiratory system in relation to energetic demand: VII. Flow of oxygen across the pulmonary gas exchanger. Respiration Physiology 6, 101–115.

Maxwell, J.C., 1873. A Treatise on Electricity and Magnetism. Dover, New York, ISBN 0-486-60637-6.

Mayo, M., Georghiu, S., Pfeifer, P., 2012. Diffusional screening in treelike spaces: an exactly solvable diffusion–reaction model. Physical Review E 85, 011115-1–011115-7.

McWhirter, J.L., Noguchi, H., Gompper, G., 2009. Flow-induced clustering and alignment of vesicles and red blood cells in microcapillaries. Proceedings of the National Academy of Sciences of the United States of America 106, 6039–6043.

Miller, G.W., Mugler III, J.P., Altes, T.A., Cai, Jing, Mata, J.F., de Lange, E.E., Tobias, W.A., Cates, G.D., Brookeman, J.R., 2010. A short-breath-hold technique for lung $pO_2$ mapping with 3He MRI. Magnetic Resonance in Medicine 63, 127–136.

Paiva, M., Engel, L.A., 1985. Model analysis of intra-acinar gas exchange. Respiration Physiology 62, 257–272.

Paiva, M., Engel, L.A., 1987. Theoretical studies of gas mixing and ventilation distribution in the lung. Physiological Reviews 67, 750–796.

Presson Jr., R.G., Hanger, C.C., Godbey, P.S., Graham, J.A., Lloyd Jr., T.C., Wagner Jr., W.W., 1994. Effect of increasing flow on distribution of pulmonary capillary transit times. Journal of Applied Physiology 76, 1701–1711.

Roughton, F.J.W., Forster, R.E., 1957. Relative importance of diffusion and chemical reaction rates in determining rate of exchange of gases in the human lung with special reference to true diffusing capacity of pulmonary membrane and volume of blood in the lung capillaries. Journal of Applied Physiology 11, 290–302.

Sapoval, B., 1994a. General formulation of Laplacian transfer across irregular surfaces. Physical Review Letters 73, 3314.

Sapoval, B. 1994. Transfer to and across irregular membranes modeled by fractal geometry. Fractals in Biology and Medicine. Nonnenmacher, T.F., Losa, G.A., Weibel, E.R., 1994.

Sapoval, B., Filoche, M., Weibel, E.R., 2001. Branched structures, acinus morphology and optimal design of mammalian lungs. In: Fleury, V., Gouyet, J.F., Leonetti, M. (Eds.), Branching in Nature. EDP Sciences/Springer Verlag, Berlin, pp. 225–242.

Sapoval, B., Weibel, E.R., Filoche, M., 2002a. Diffusion screening, acinus size and optimal design of mammalian lungs. In: Losa, G.A., Merlini, D., Nonennmacher, T.F., Weibel, E.R. (Eds.), Fractals in biology and medicine, vol. II. Birhauser, Basel, pp. 25–38.

Sapoval, B., Filoche, M., Weibel, E.R., 2002b. Smaller is better-but not too small: a physical scale for the design of the mammalian pulmonary acinus. Proceedings of the National Academy of Sciences of the United States of America 99, 10411–10416.

Sapoval, B., Filoche, M., 2008. Role of diffusion screening in pulmonary diseases. Integration in Respiratory Control: From Genes to Systems 605, 173–178.

Scheid, P., Piiper, J., 1980. Intrapulmonary gas mixing and stratification. Pulmonary Gas Exchange 1, 87–130.

Scheid, P., Piiper, J., 1989. Blood gas equilibration in lungs and pulmonary diffusing capacity. In: Chang, H.K., Païva, M. (Eds.), Respiratory Physiology, vol. 40. Dekker, New York, Basel, pp. 453–497.

Swan, A.J., Tawhai, M.H., 2011. Evidence for minimal oxygen heterogeneity in the healthy human pulmonary acinus. Journal of Applied Physiology 110, 528–537.

Tamhane, R.M., Johnson Jr., R.L., Hsia, C.C.W., 2001. Pulmonary membrane diffusing capacity and capillary blood volume measured during exercize from nitric oxide uptake. Chest 125, 1019–1027.

Tawhai, M.H., Hunter, P.J., 2001. Characterizing respiratory airway gas mixing using a lumped parameter model of the pulmonary acinus. Respiration Physiology Vol127, 241–248.

Tsuda, A., Henry, F.S., Butler, J.P., 1995. Chaotic mixing of alveolated duct flow in rythmically expanding pulmonary acinus. Journal of Applied Physiology 79, 1055–1063.

Vaughn, M.W., Huang, K.T., Kuo, L., Liao, J.C., 2000. Erythrocytes possess an intrinisc barrier to nitic oxide. Journal of Biological Chemistry 275, 2342–2348.

Vock, R., Weibel, E.R., 1993. Massive hemorrhage causes changes in morphometric parameters of lung capillaries and concentration of leukocytes in microvasculature. Experimental Lung Research 19, 559–577.

Watson, J., Kamm, R.D., Burwen, D.R., Brown, R., Ingenito, E., Slutsky, A.S., 1987. Gas exchange during constant flow ventilation with different gases. American Review of Respiratory Disease 136, 420–425.

Weibel, E.R., Taylor, C.R., Gehr, P., Hoppeler, H., Mathieu, O., Maloiy, G.M.O., 1981. Design of the mammalian respiratory system IX. Functional and structural limits for oxygen flow. Respiration Physiology 44, 151–164.

Weibel, E.R., 1984. The Pathway for Oxygen. Harvard University Press, Cambridge, MA.

Weibel, E.R., Federspiel, W.J., Fryder-Doffey, F., Hsia, C.C., Konig, M., Stalder-Navarro, V., Vock, R., 1993. Morphometric model for pulmonary diffusing capacity I. Membrane diffusing capacity. Respiration Physiology 93, 125–149.

Weibel, E.R., Sapoval, B., Filoche, M., 2005. Design of peripheral airways for efficient gas exchange. Respiratory Physiology & Neurobiology 148, 3–21.
West, J.W., 2008. Respiratory Physiology: The Essentials, 8th ed. Wolters Kluwer/Lippincott Williams & Wilkins, Baltimore, Philadelphia.
Yamaguchi, K., Nguyen-Phu, D., Scheid, P., Piiper, J., 1985. Kinetics of $O_2$ uptake and release by human erythrocytes studied by a stopped-flow technique. Journal of Applied Physiology 58, 1215–1224.
Zavorsky, G.S., Quiron, K.B., Massarelli, P.S.P., Lands, L.C., 2004. The relationship between single-breath diffusion capacity of the lung for nitric oxide and carbon monoxide during various exercize intensities. Chest 125, 1019–1027.
Zavorsky, G.S., Murias, J.M., 2006. A small amount of inhaled nitric oxide does not increase lung diffusing capacity. European Respiratory Journal 27, 1251–1257.